# Dephasing in the electronic Mach-Zehnder interferometer at filling factor $\nu=2$

Levkivskyi, Ivan; Sukhorukov, Eugene

**How to cite**

LEVKIVSKYI, Ivan, SUKHORUKOV, Eugene. Dephasing in the electronic Mach-Zehnder interferometer at filling factor $\nu=2$. In: Physical review. B, Condensed matter and materials physics, 2008, vol. 78, n° 4. doi: 10.1103/PhysRevB.78.045322

This publication URL: https://archive-ouverte.unige.ch/unige:36341
Publication DOI: 10.1103/PhysRevB.78.045322

# Dephasing in the electronic Mach-Zehnder interferometer at filling factor $\nu=2$

Ivan P. Levkivskyi[1,2] and Eugene V. Sukhorukov[1]
[1]*Département de Physique Théorique, Université de Genève, CH-1211 Genève 4, Switzerland*
[2]*Physics Department, Kyiv National University, 03022 Kyiv, Ukraine*
(Received 18 January 2008; revised manuscript received 13 May 2008; published 31 July 2008)

We propose a simple physical model which describes dephasing in the electronic Mach-Zehnder interferometer at filling factor $\nu=2$. This model explains very recent experimental results, such as the unusual lobe-type structure in the visibility of Aharonov-Bohm oscillations, phase rigidity, and the asymmetry of the visibility as a function of transparencies of quantum point contacts. According to our model, dephasing in the interferometer originates from strong Coulomb interaction at the edge of two-dimensional electron gas. The long-range character of the interaction leads to a separation of the spectrum of edge excitations on slow and fast mode. These modes are excited by electron tunneling and carry away the phase information. The new energy scale associated with the slow mode determines the temperature dependence of the visibility and the period of its oscillations as a function of voltage bias. Moreover, the variation of the lobe structure from one experiment to another is explained by specific charging effects, which are different in all experiments. We propose to use a strongly asymmetric Mach-Zehnder interferometer with one arm being much shorter than the other for the spectroscopy of quantum Hall edge states.

DOI: 10.1103/PhysRevB.78.045322 PACS number(s): 73.23.−b, 03.65.Yz, 85.35.Ds

## I. INTRODUCTION

The quantum Hall effect (QHE),[1] one of the central subjects of the modern mesoscopic physics,[2] continues to attract an attention of both experimentalists and theorists. It is well known that the low-energy physics of the QHE at the Hall plateau is determined by the edge excitations because at strong magnetic fields, there exists a gap for excitations in the bulk of the two-dimensional electron gas (2DEG). Properties of quantum Hall edge excitations were investigated in a number of experimental and theoretical works.[3] However, only very recently the progress in the fabrication of novel mesoscopic systems made it possible to closely focus on the electronic properties of quantum Hall edge, which were not well understood earlier. In particular, experiments on the quantum interference and dephasing processes in electronic Mach-Zehnder[4] interferometers (MZI) brought remarkable results, which shed light on new physics of quantum Hall edge states. This physics is the subject of our theoretical investigation.

The idea of the electronic MZI is the same in all recent experiments.[5–10] The region of the sample, where the 2DEG is present, is topologically equivalent to so called *Corbino disk* (see Fig. 1). There are at least two ohmic contacts: one is grounded and the second is biased by the potential difference $\Delta\mu$. The current $I$ is detected at one of the ohmic contacts. In fact, experiments that we discuss used several ohmic contacts for the convenience of the measurement, although only two contacts are required for the realization of MZI. Two quantum point contacts (QPCs) play a role of beam splitters, which mix outer edge channels (thin black line in Fig. 1). The inner channels, blue (gray) lines in Fig. 1, are *always* reflected from QPCs.

Typically, the transparencies of two QPCs were varied between $T_\ell=0$ and $T_\ell=1$, $\ell=L,R$. However, the most interesting physics was observed in two limits: in the regimes of weak tunneling $T_\ell\to 0$ and of weak backscattering $T_\ell\to 1$. In the first regime one of the outer channels is biased (upper channel in Fig. 1) and almost completely reflected at the first QPC. Then it runs on the same (upper) part of the Corbino disk. The channel that originates from the second (lower) ohmic contact is grounded. In the second regime (shown in Fig. 1 as example) the biased channels are almost fully transmitted at the first QPC to the opposite (lower) part of the Corbino disk. The physical consequences of the difference between these two regimes will be discussed later in Sec. IV.

Two ohmic contacts are connected solely via scattering at two QPCs. Consequently, there are two paths between ohmic contacts, which contribute to the total current $I$. The first path is reflected at the right QPC and transmitted at the left one,

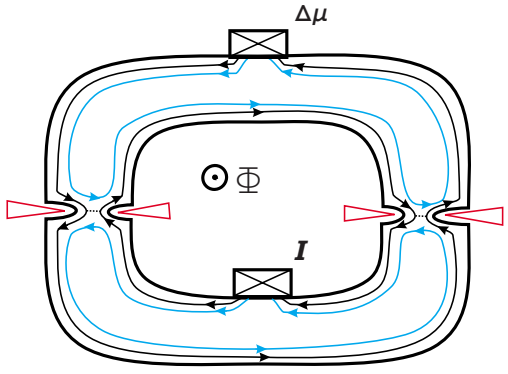


FIG. 1. (Color online) The Mach-Zehnder interferometer is schematically shown as a Corbino disk, which contains the two-dimensional electron gas (2DEG). In strong magnetic field at filling factor $\nu=2$ two chiral one-dimensional channels are formed and propagate along the edge of 2DEG. Inner channels, blue (gray) lines, are *always* reflected from both quantum point contacts (QPC), while outer channels, black lines, are mixed by QPCs. Bias $\Delta\mu$ applied to the upper ohmic contact causes the current $I$ to flow to the lower ohmic contact. This current is due to scattering at QPCs and contains the interference contribution sensitive to the magnetic flux $\Phi$ and leading to Aharonov-Bohm oscillations.

 

while it is the other way around for the second path. It is easy to see that two paths enclose a loop with the nonzero magnetic flux. The Aharonov-Bohm (AB) phase associated with it may be changed either by varying slightly the strength of the magnetic field, or by varying the length of one of the paths with the help of the modulation gate placed near the corresponding arm of the interferometer.

According to a frequently used single-particle picture,[2] the electron edge states propagate as plane waves with the group velocity $v_F$ at Fermi level. They are transmitted through the MZI (see Fig. 1) at the left and right QPCs with amplitudes $t_L$ and $t_R$, respectively. In the case of low transmission, two amplitudes add so that the total transmission probability oscillates as a function of the AB phase $\varphi_{\mathrm{AB}}$ and bias $\Delta\mu$. The visibility of the oscillations of the differential conductance $\mathcal{G} \equiv dI/d\Delta\mu$ is defined as

$$V_{\mathcal{G}} = \frac{\mathcal{G}_{\max} - \mathcal{G}_{\min}}{\mathcal{G}_{\max} + \mathcal{G}_{\min}}. \tag{1}$$

Then the Landauer-Büttiker formula[11] applied to the differential conductance gives the following result for the visibility and the AB phase shift:

$$V_{\mathcal{G}} = \frac{2|t_L t_R|}{|t_L|^2 + |t_R|^2}, \quad \Delta\varphi_{\mathrm{AB}} = \frac{\Delta L}{v_F}\Delta\mu, \tag{2}$$

where $\Delta L$ is the length difference between two paths of the MZI. Thus we arrive at the result that in the absence of interaction the visibility is independent of bias, while phase shift grows linearly with bias.

The most interesting observation made in experiments[5–9] is that the simple single-particle picture of edge states fails to correctly describe the AB effect in the MZI. Essentially, the results can be summarized as following: The visibility of AB oscillations is not constant, but rather strongly depends on bias $\Delta\mu$. It oscillates, showing a new energy scale, and may vanish at specific values of bias. While this behavior is observed in all experiments, the details are different and important for understanding the underlying physics. Therefore, we group experimental observations roughly in two parts, according to a specific important feature of the experimental setup, and describe them below in details.

### A. Only one edge channel is biased

The first experimental situation that we wish to address is reported in Ref. 5. In this experiment the bias is applied to the outer channel only. This situation is achieved by splitting incoming inner and outer channels with the help of an additional QPC, so that two channels originate in fact from different ohmic contacts. This allows a different bias to be applied separately to two channels at the same edge.

The MZI in this situation is schematically shown in Fig. 2 for the regimes of weak tunneling $T_\ell \to 0$ (left panel), and of weak backscattering $T_\ell \to 1$ (right panel). This schematic is obtained from Fig. 1 by splitting each ohmic contact attached to the Corbino disk and deforming two interfering paths so that they run from left to right. After this procedure, the symmetry between two scattering regimes becomes obvious:

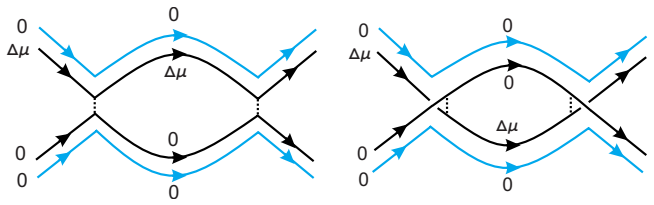


FIG. 2. (Color online) Schematic representation of the experimental setup in Ref. 5. Only one edge channel of the MZI is biased. Left panel shows the *weak tunneling* regime: Outer edge channels that propagate at different arms of the MZI are weakly coupled to each other at two QPCs. Right panel shows the *weak backscattering* regime: Outer edge channels almost completely propagate through QPCs to opposite arms of the MZI and only weakly coupled via backscattering.

In order to go from the setup on the left panel of Fig. 2 to the one on the right panel, one needs to simply flip the interferometer vertically. This symmetry is important, and will be shown in Sec. IV to result in the symmetry between weak tunneling and weak backscattering regimes.

Reference 5 discovered an unexpected AB effect which is inconsistent with the single-particle picture of edge channels. The following observations where reported: (1) lobe-type structure in the dependence of the visibility of AB oscillations on the dc bias with almost equal widths of lobes. The visibility vanishes at specific values of the bias. This behavior persists for various fixed values of magnetic field and for various transparencies of QPCs; (2) the rigidity of the AB phase shift followed by sharp $\pi$-valued jumps at the points where the visibility vanishes; and (3) the stability of both mentioned effects with respect to changes in the length of one of the interferometer paths.

The experiment[5] was theoretically analyzed in several recent works.[12–15] Reference 12 focuses on $\nu=1$ case and suggests that the suppression of the visibility is due to the resonant interaction with the counter-propagating edge channel located near one of the arms of the interferometer.[16] This idea may correctly describe dephasing at $\nu=1$ in this specific case. However, the experiments of Refs. 5 and 6 concentrate on the $\nu=2$ regime, where two edge channels coexist. These and new experiments,[7–9] where the counter-propagating edge channel has been removed, prompt a new theoretical analysis. The authors of Ref. 13 consider a long-range Coulomb interaction at the edge and make an interesting prediction about the temperature dependence of the visibility. However, they are not able to propose an explanation of the lobe-type behavior of the visibility. References 14 and 15 suggest that dephasing in MZI is due to shot noise generated by the partition of the edge channel at the first QPC. While this idea may correctly capture a part of the physics at $\nu=1$, the drawback of this explanation is that the shot noise vanishes in weak tunneling and weak backscattering regimes, where the experiments nevertheless demonstrate strong dephasing. Moreover, the experiment which we discuss below illuminates the special role that the second inner edge channel at $\nu=2$ plays in dephasing.

### B. Two edge channels are biased

In contrast to the work,[5] the experimental setup in Ref. 6 does not contain an additional QPC that would allow to split

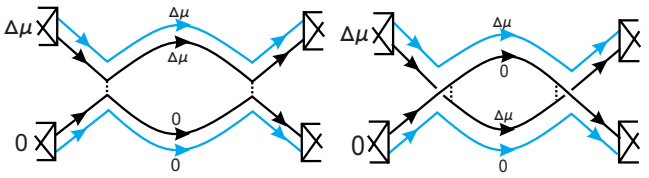


FIG. 3. (Color online) Schematic representation of the experimental setup in Ref. 6. Two incoming edge channels of the MZI are biased with the same potential difference $\Delta\mu$, and other channels are grounded. Left panel shows the *weak tunneling* regime, while the right panel shows the *weak backscattering* regime.

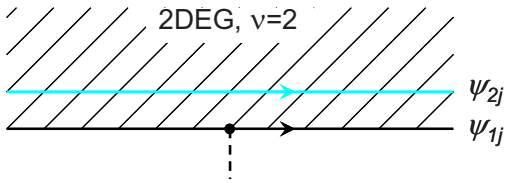


FIG. 4. (Color online) Structure of the quantum Hall edge at $\nu=2$. Two chiral electrons, $\psi_{1j}$ and $\psi_{2j}$, are propagating along the edge. Tunneling is possible only from and to the outer channel ($\psi_{1j}$, black line).

two edge channels at $\nu=2$ and to apply potentials to each of them separately. Therefore, in Ref. 6 two edge channels that originate from the same ohmic contact are biased by the same potential difference $\Delta\mu$. For the convenience of the following analysis we again unfold the MZI on Fig. 1 and represent it schematically as shown in Fig. 3.

Now it is easy to see the asymmetry between regimes of weak tunneling and of weak backscattering. In the first regime (left panel) two channels on the upper arm of the interferometer are equally biased with the potential difference $\Delta\mu$. The situation is different in the second regime (right panel): The inner channel is biased on the upper arm of the interferometer, while the outer channel is biased on the lower arm. We believe that this asymmetry is responsible for entirely different behavior of the visibility of AB oscillations in the experiment:[6] (1) Lobe-type structure with the visibility vanishing at certain values of bias is observed only in the weak tunneling regime. The central lobe is approximately two times wider than the side lobes. In the weak backscattering regime the visibility shows oscillations and decays as a function of the bias. (2) No phase rigidity is found at all transparencies of QPCs. (3) The asymmetry in the visibility as a function of the transparency of the first QPC is observed. In particular, the visibility always decays as a function of the bias in the regimes of weak tunneling. In contrast, in the regime of weak backscattering the visibility first grows around zero bias, and only then it decays.

It is the last observation which is very important. It indicates that charging effects induced by different biasing of edge channels may be responsible for differences in the results of experiments of Refs. 5 and 6 This idea seems to agree with the conclusion of the authors[17] of the experiment.[7] In this paper we develop this idea and propose a simple model that is capable to explain on a single basis all the experimental observations described above. Namely, we assume a strong (Coulomb) interaction between two edge channels that belong to the same quantum Hall edge. The interaction effect is complex: First of all, it leads to charging of edge channels and induces experimentally observed phase shifts. Second, the interaction is partially screened, which leads to the emergence of the soft mode and of a new low-energy scale associated with it. The width of lobes in the visibility and the temperature dependence are determined by this energy scale. Finally, the interaction is responsible for the decay of coherence at large bias.

Further details of our model are given in Sec. II, while in Appendix A we check the consistency of the model. In Sec. III we express the visibility of AB oscillations in terms of electronic correlation functions, and derive these functions in Appendix B. In Sec. IV we present a detailed comparison of our results with the experimental observations. Finally, in Sec. V we briefly summarize our results.

## II. MODEL OF MACH-ZEHNDER INTERFEROMETER

Before we proceed with the mathematical formulation of the model we wish to stress the following points. The experimentally found new energy scale[5–9] is very small. For instance, the width of lobes in the visibility is approximately 20 $\mu$V. We show below that this energy is inversely proportional to the size of the MZI, which is a few micrometers. Thus it is much smaller than any other energy scale associated, e.g., with the formation of compressible strips.[18] Therefore, we use an effective model[19] appropriate for the description of the low-energy physics of quantum Hall edge excitations. Namely, we consider the inner and outer edge channels at $\nu=2$ as two chiral boson fields and introduce the Luttinger-type Hamiltonian[3,20] to describe the equilibrium state. Second, we introduce the density-density interaction, which is known to be irrelevant in the low-energy limit.[19] This fact has no influence on the physics that we discuss below because we focus on the processes at finite energy and length scale, which take place inside the MZI.

### A. Fields and Hamiltonian

We assume that at filling factor $\nu=2$ there are two edge channels at each edge of the quantum Hall system and two chiral fermions associated with them and denoted by: $\psi_{\alpha j}(x)$, $\alpha=1,2$, and $j=U,D$. Here the subscript 1 corresponds to the fermion on the outer channel, and 2 to the fermion on the inner channel (see Fig. 4), while the index $j$ stands for the upper and lower arms of the interferometer. The total Hamiltonian of the interferometer

$$\mathcal{H}_{\text{tot}} = \mathcal{H}_0 + \mathcal{H}_{\text{int}} + \mathcal{H}_T \tag{3}$$

contains single-particle term $\mathcal{H}_0$, interaction part $\mathcal{H}_{\text{int}}$, and the tunneling Hamiltonian $\mathcal{H}_T$.

The single-particle Hamiltonian describes free chiral fermions:[19]

$$\mathcal{H}_0 = -iv_F \sum_{\alpha,j} \int dx \psi^\dagger_{\alpha j} \partial_x \psi_{\alpha j}, \tag{4}$$

where $v_F$ is a Fermi velocity, which is assumed to be the same for each edge channel. This assumption is not critical

because as we will see below, the Fermi velocity is strongly renormalized by the interaction.

We postpone for a while a detailed discussion of the interaction and at the moment write the interaction Hamiltonian in terms of local densities $\rho_{\alpha j}$ in the following general form:

$$\mathcal{H}_{\rm int} = (1/2)\sum_{\alpha,\beta,j}\int\int dxdy U_{\alpha\beta}(x-y)\rho_{\alpha j}(x)\rho_{\beta j}(y). \quad (5)$$

Note that this effective Hamiltonian is not microscopically derived. However, the experiment indicates[17] that the interaction has a Coulomb long-range character and leads to charging effects at the edge. Below we show that once this assumption is made, it leads to a number of universalities in the MZI physics and correctly captures most of the experimental observations.

We have already mentioned in Sec. I that the interference in MZI originates from scattering processes at QPCs. In the case when interaction is strong, the scattering has to be assumed weak and treated perturbatively. Fortunately, this limitation does not detract from our theoretical approach because neither the interference nor its suppression is necessarily weak in the case of weak scattering. Moreover, we would like to stress again that most interesting physics takes place in the regimes of weak tunneling and of weak backscattering.

Both regimes can be described by the tunneling Hamiltonian

$$\mathcal{H}_T = A + A^\dagger \equiv \sum_\ell (A_\ell + A_\ell^\dagger), \quad \ell = L,R, \quad (6)$$

where the tunneling amplitude

$$A_\ell = t_\ell \psi_{1D}^\dagger(x_\ell)\psi_{1U}(x_\ell) \quad (7)$$

connects outer edge channels and transfers the electron from the lower arm to the upper arm of the MZI. It is worth mentioning already here that at low energies the electron tunneling is relevant and leads in fact to the ohmic behavior of the QPCs, in agreement with experiments.[5,6] The AB phase may now be included in the tunneling amplitudes via the relation $t_R^* t_L = |t_R t_L| e^{i\varphi_{\rm AB}}$.

### B. Bosonization

In order to account for the strong interaction at the edge, we take advantage of the commonly used bosonization technique,[20] and represent fermion operators in terms of chiral boson fields $\phi_{\alpha j}$:

$$\psi_{\alpha j} \propto e^{i\phi_{\alpha j}}, \quad (8)$$

which satisfy the commutation relations $[\phi_{\alpha j}(x), \phi_{\alpha j}(y)] = i\pi\,\mathrm{sgn}(x-y)$. The local density is obtained via the point splitting

$$\rho_{\alpha j}(x) = \lim_{\varepsilon\to 0} \psi_{\alpha j}^\dagger(x+\varepsilon)\psi_{\alpha j}(x),$$

which gives the following expression:

$$\rho_{\alpha j}(x) = (1/2\pi)\partial_x \phi_{\alpha j}(x). \quad (9)$$

Applying point splitting to the single-particle Hamiltonian [Eq. (4)], we obtain

$$\mathcal{H} \equiv \mathcal{H}_0 + \mathcal{H}_{\rm int} = \sum_{\alpha,\beta,j}\int\int \frac{dxdy}{8\pi^2} \times V_{\alpha\beta}(x-y)\partial_x\phi_{\alpha j}(x)\partial_y\phi_{\beta j}(y), \quad (10)$$

where the interaction potential is simply shifted by the Fermi velocity

$$V_{\alpha\beta} = U_{\alpha\beta} + 2\pi v_F \delta_{\alpha\beta}\delta(x-y). \quad (11)$$

The crucial point is that now the Hamiltonian [Eq. (10)] for quantum Hall edge is quadratic in boson fields.

Next, we quantize fields by expressing them in terms of boson creation and annihilation operators, $a_{\alpha j}^\dagger(k)$ and $a_{\alpha j}(k)$,

$$\phi_{\alpha j}(x) = \varphi_{\alpha j} + 2\pi p_{\alpha j} x + \sum_{k>0}\sqrt{\frac{2\pi}{Wk}}[a_{\alpha j}(k)e^{ikx} + a_{\alpha j}^\dagger(k)e^{-ikx}], \quad (12)$$

where zero modes $\varphi_{\alpha j}$ and $p_{\alpha j}$ satisfy commutation relations $[p_{\alpha j}, \varphi_{\alpha j}] = i/W$, and $W$ is the total size of the system. In the end of the calculations we take the thermodynamic limit $W\to\infty$ so that $W$ drops from the final result. Then the edge Hamiltonian acquires the following form:

$$\mathcal{H} = (1/2\pi)\sum_{\alpha,\beta,j,k} kV_{\alpha\beta}(k)a_{\alpha j}^\dagger(k)a_{\beta j}(k) + (W/2)\sum_{\alpha,\beta,j} V_{\alpha\beta}(0)p_{\alpha j}p_{\beta j}. \quad (13)$$

The vacuum for collective excitations is defined as $a_{\alpha j}(k)|0\rangle = 0$. Special care has to be taken about zero modes because as we show in Sec. IV, zero modes determine charging effects and phase shifts, which are not small. From the definitions (9) and (12) it is clear that the zero mode $p_{\alpha j}$ has a meaning of a homogeneous density at the edge channel $(\alpha, j)$. Therefore, we define "vacuum charges" $Q_{\alpha j}$ as

$$p_{\alpha j}|0\rangle = Q_{\alpha j}|0\rangle, \quad (14)$$

which are in fact charge densities at the edge channels, generated by the bias. The energy $E_0$ of the ground state, defined as $\mathcal{H}|0\rangle = E_0|0\rangle$, is then given by

$$E_0 = (W/2)\sum_{\alpha,\beta,j} V_{\alpha\beta}(0)Q_{\alpha j}Q_{\beta j}. \quad (15)$$

Since edge excitations propagate along the equipotential lines, edge channels can be considered metallic surfaces. We therefore can apply the well-known electrostatic relation[21] for the potentials $\Delta\mu_{\alpha j}$ to the edge channels:

$$\Delta\mu_{\alpha j} \equiv (1/W)\delta E_0/\delta Q_{\alpha j} = \sum_\beta V_{\alpha\beta}(0)Q_{\beta j}. \quad (16)$$

Thus the quantity $V_{\alpha\beta}(0)$ is the inverse capacitance matrix.[22] Using now Eqs. (13) and (14), and the commutation relation for zero modes, we arrive at the following important result for the time evolution of zero modes:

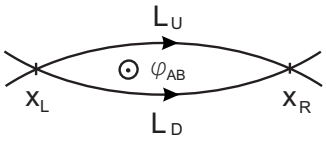


FIG. 5. Schematics of MZI introducing notations: $L_U$ and $L_D$ are the lengths of the upper and lower paths of the interferometer, respectively. The coordinates of the left and right QPC are denoted by $x_L$ and $x_R$, respectively. The magnetic flux threading the interferometer results in the AB phase $\varphi_{\mathrm{AB}}$.

$$Q_{\alpha j}(t) = \sum_{\beta} V^{-1}_{\alpha\beta}(0)\Delta\mu_{\beta j}, \quad \varphi_{\alpha j}(t) = -\Delta\mu_{\alpha j} t. \tag{17}$$

We finally note that the formulated model here of the MZI is consistent with the effective theory of the quantum Hall state[19] at $\nu=2$. This is demonstrated in Appendix A, where we check the locality of the electron operators, their fermionic commutation relations, and the gauge invariance of our model.

### C. Strong interaction limit and the universality

It is quite natural to assume that edge channels interact via the Coulomb potential. It has a long-range character and the logarithmic dispersion $V_{\alpha\beta}(k) \propto \log(ka)$. Here $a$ is the shortest important length scale, e.g., the width of compressible stripes,[18] or the interchannel distance. The dispersion is important in the case $\nu=1$ because it generates dephasing at the homogeneous edge.[13] However, taken alone the dispersion is not able to explain lobe-type behavior of the visibility. What is more important is the fact that the logarithm may become relatively large when cutoff occurs at relevant long distances.

We therefore further assume that the Coulomb interaction is screened at distances $D$, such as $L_U, L_D \gg D \gg a$, where $L_U$ and $L_D$ are the lengths of the arms of the MZI (see Fig. 5). In fact, some sort of screening may exist in MZIs. For instance, in the experiments[5–9] the cutoff length $D$ may be a distance to the back gate or to the massive metallic air bridge. There are several consequences of screening on the intermediate distances $D$. First of all, it allows to neglect the interaction between the two arms of the interferometer (see however the discussion in Sec. IV). Second, at low energies we can neglect the logarithmic dispersion and write

$$V_{\alpha\beta}(x-y) = V_{\alpha\beta}\delta(x-y), \tag{18}$$

so that for the Fourier transform we obtain $V_{\alpha\beta}(k)=V_{\alpha\beta}(0) \equiv V_{\alpha\beta}$. Finally, the mutual interaction between inner and outer edge channels, located on the distance of order $a \ll D$ from each other, is strongly reduced.

Therefore, one can parametrize the interaction matrix as follows:

$$V_{\alpha\beta} = \pi \begin{pmatrix} u+v & u-v \\ u-v & u+v \end{pmatrix}, \tag{19}$$

where

$$u/v = \log(D/a) \gg 1 \tag{20}$$

is a new large parameter, the most important consequence of the long-range character of Coulomb interaction.

Indeed, we now diagonalize the interaction, $V=S^{\dagger}\Lambda S$, with the result

$$\Lambda = 2\pi \begin{pmatrix} u & 0 \\ 0 & v \end{pmatrix}, \quad S = \frac{1}{\sqrt{2}} \begin{pmatrix} 1 & 1 \\ 1 & -1 \end{pmatrix}. \tag{21}$$

Thus we find that the Coulomb interaction at the $\nu=2$ edge leads to the separation of spectrum on the fast (charge) mode with the speed $u$ and slow (dipole) mode with the speed $v$. In Sec. IV we show that the lobe structure in the visibility is determined by the slow mode, while the fast mode is not excited at relevant low energies. That is why at $\nu=2$ the logarithmic dispersion of the Coulomb interaction is not important for explaining lobes.

Moreover, the Coulomb character of the interaction leads to the following universality. We show later that the coupling of electrons in the outer channel to the fast and slow mode is determined by the parameters $s_\alpha=|S_{1\alpha}|^2$, which satisfy the sum rule

$$\sum_{\alpha} s_\alpha = \sum_{\alpha} |S_{1\alpha}|^2 = 1 \tag{22}$$

that follows from the unitarity of the matrix $S$. For the special choice [Eq. (19)] of the interaction matrix coupling constants are equal,

$$s_1 = s_2 = 1/2, \tag{23}$$

which has an important consequence, as we will show in Sec. III. Note that in the limit of strong long-range interaction, $u \gg v_F$, the result [Eq. (23)] is stable against variations of the bare Fermi velocity $v_F$ and is not sensitive to the physics of edge channels at distances of order $a$, leading to the universality of dephasing in MZI.

Finally, we partially diagonalize the Hamiltonian by introducing new boson operators via $a_{\alpha j}(k)=\Sigma_\beta S_{\alpha\beta} b_{\beta j}(k)$. Using Eqs. (13), (19), and (21), we obtain new Hamiltonian for the quantum Hall edge

$$\mathcal{H} = \sum_{j,k} [uk b^{\dagger}_{1j}(k) b_{1j}(k) + vk b^{\dagger}_{2j}(k) b_{2j}(k)] + (W/2) \sum_{\alpha,\beta,j} V_{\alpha\beta} p_{\alpha j} p_{\beta j}, \tag{24}$$

which completes our discussion of the model. In Appendix B we use Eqs. (8), (12), (17), and (24) to derive electronic correlation functions.

## III. VISIBILITY AND PHASE SHIFT

In this section we consider the transport through the MZIs shown in Figs. 1–3 and evaluate the visibility of AB oscillations. Both regimes of weak tunneling and of weak backscattering can be considered on the same basis, by applying the tunneling Hamiltonian approach.[23] In the derivation presented below we follow Ref. 12. We introduce the tunneling

current operator $\hat{I}=\dot{N}_D=i[\mathcal{H}_T,N_D]$, which differs for two regimes only by sign. Here $N_D=\int dx\psi_{1D}^\dagger\psi_{1D}$ is the number of electrons on the outer edge channel of the lower arm of the interferometer. Then we use Eqs. (6) and (7) to write

$$\hat{I}=i(A^\dagger-A). \tag{25}$$

We evaluate the average current to lowest order in tunneling and obtain

$$I=\int_{-\infty}^{\infty}dt\langle[A^\dagger(t),A(0)]\rangle, \tag{26}$$

where the average is taken with respect to ground state in quantum Hall edges. Finite temperature effects will be considered separately in Sec. IV C.

It easy to see that the average current can be written as a sum of four terms:

$$I=\sum_{\ell,\ell'}I_{\ell\ell'},\quad I_{\ell\ell'}\equiv\int dt\langle[A_\ell^\dagger(t),A_{\ell'}(0)]\rangle, \tag{27}$$

where $I_{LL}$ and $I_{RR}$ are the direct currents at the left and right QPC, respectively, and $I_{LR}+I_{RL}$ is the interference contribution. In our model there is no interaction between the upper and lower arms of MZI, therefore the correlation function in Eq. (27) splits into the product of two single-particle correlators:

$$I_{\ell\ell'}=t_\ell^*t_{\ell'}\int dt[\langle\psi_{1U}^\dagger(x_\ell,t)\psi_{1U}(x_{\ell'},0)\rangle\langle\psi_{1D}(x_\ell,t)\psi_{1D}^\dagger(x_{\ell'},0)\rangle - \langle\psi_{1U}(x_{\ell'},0)\psi_{1U}^\dagger(x_\ell,t)\rangle\langle\psi_{1D}^\dagger(x_{\ell'},0)\psi_{1D}(x_\ell,t)\rangle]. \tag{28}$$

We note that the operator $\psi_{1j}^\dagger$ applied to the ground state creates a quasiparticle above the Fermi level (with the positive energy), while the operator $\psi_{1j}$ creates a hole below Fermi level (with the negative energy). This implies that in the first term of Eq. (28) all the singularities are shifted to the upper half plane of the complex variable $t$, and in the second term singularities are shifted to the lower half plane. This means that only one term contributes, depending on the sign of bias $\Delta\mu$, which determines the direction of current. Apart from this, there is no difference between the two terms. Therefore, we choose, e.g., the first term, shift the counter of integration $C$ to the low half plane, and rewrite expression (28) as follows:

$$I_{\ell\ell'}=t_\ell^*t_{\ell'}\int_C dt\langle\psi_{1U}^\dagger(x_\ell,t)\psi_{1U}(x_{\ell'},0)\rangle\times\langle\psi_{1D}^\dagger(x_\ell,t)\psi_{1D}(x_{\ell'},0)\rangle^*, \tag{29}$$

where the correlators are defined in such a way that they have singularities on the real axis of $t$.

The correlators are evaluated in Appendix B using the bosonization technique with the result

$$i\langle\psi_{1j}^\dagger(x_\ell,t)\psi_{1j}(x_{\ell'},0)\rangle=\frac{\exp[i\Delta\mu_{1j}t-2\pi iQ_{1j}(x_\ell-x_{\ell'})]}{(x_\ell-x_{\ell'}-ut)^{s_1}(x_\ell-x_{\ell'}-vt)^{s_2}}. \tag{30}$$

One important fact we will prove below is that for $x_\ell=x_{\ell'}$, the only role of the interaction is to renormalize the density of states at Fermi level, $n_F=1/(u^{s_1}v^{s_2})$. This immediately follows from the sum rule [Eq. (22)]. Therefore, for the direct currents we readily obtain

$$I_{\ell\ell}=2\pi n_F^2|t_\ell|^2\Delta\mu, \tag{31}$$

i.e., the QPCs are in the ohmic regime, in agreement with experimental observations.

In order to present the visibility in a compact form, we introduce the electron correlation functions of an isolated edge, normalized to the density of states,

$$G_j(t)=\frac{\exp[2\pi iQ_{1j}L_j]}{(t-L_j/u)^{s_1}(t-L_j/v)^{s_2}},\quad j=U,D. \tag{32}$$

These functions contain all the important information about charging effects (phase shift generated by zero modes) and dephasing determined by the singularities. Next, adding all the terms $I=\Sigma I_{\ell\ell'}$ we find the differential conductance $\mathcal{G}=dI/d\Delta\mu$:

$$\mathcal{G}=2\pi n_F^2(|t_L|^2+|t_R|^2)+2n_F^2|t_Lt_R|\mathrm{Im}\left\{e^{i\varphi_{\mathrm{AB}}}\int_C dte^{i\Delta\mu t}(t-\Delta t)G_U^*(t)G_D(t)\right\}, \tag{33}$$

where the time shift $\Delta t$ is the charging effect

$$\Delta t=2\pi\partial_{\Delta\mu}(Q_{1U}L_U-Q_{1D}L_D), \tag{34}$$

which depends on the bias scheme, and will be calculated in Sec. IV for particular experimental situations. It is important to note that in the weak backscattering regime (see Figs. 2 and 3) tunneling occurs from the lower arm of the interferometer, therefore one should exchange indexes $U$ and $D$.

The first term in Eq. (33) is the contribution of direct incoherent currents through QPCs, while the second term is the interference contribution, which oscillates with magnetic field. Therefore, the visibility of AB oscillations [Eq. (1)] in the differential conductance $\mathcal{G}$ and the AB phase shift take the following form:

$$V_{\mathcal{G}}(\Delta\mu)=V_{\mathcal{G}}(0)|\mathcal{I}_{\mathrm{AB}}|,\quad \Delta\varphi_{\mathrm{AB}}=\arg(\mathcal{I}_{\mathrm{AB}}), \tag{35}$$

where the visibility at zero bias $V_{\mathcal{G}}(0)$ is given by Eq. (2) for a noninteracting system, while all the interaction effects enter via the dimensionless Fourier integral

$$\mathcal{I}_{\mathrm{AB}}(\Delta\mu)=\int_C\frac{dt}{2\pi i}\exp(i\Delta\mu t)(t-\Delta t)G_U^*(t)G_D(t), \tag{36}$$

with the counter $C$ shifted to the lower half plane of the variable $t$. This formula, together with Eqs. (32) and (34), is one of the central results and will serve as a starting point for the analysis of experiments. However, before we proceed

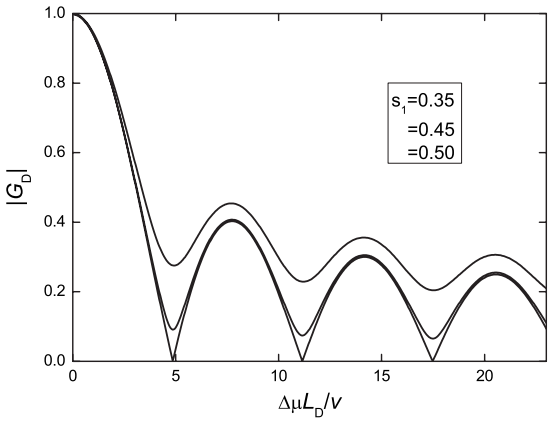


FIG. 6. The absolute value of the Fourier transform of the electronic correlation function $G_D(t)$ plotted as a function of the dimensionless bias $\Delta\mu L_D/v$ for different values of the coupling coefficient $s_1$.

with detailed explanations of experiments, we would like to quickly consider two examples.

The first example, a noninteracting system serves merely as a test for our theory. In this case using relevant parameters, the vacuum charges $Q_{1U}=\Delta\mu/v_F$, $Q_{1D}=0$, the group velocities $u=v=v_F$, coupling constants $s_1=1$, $s_2=0$, we obtain the correlators $G_U(t)=(t-L_U/v_F)^{-1}\exp(i\Delta\mu L_U/v_F)$ and $G_D(t)=(t-L_D/v_F)^{-1}$. The time shift $\Delta t=L_U/v_F$ follows from Eq. (34). We substitute all these results to the Eq. (36) and finally obtain

$$\mathcal{I}_{\mathrm{AB}}=\int_C \frac{dt}{2\pi i}\frac{e^{i\Delta\mu(t-L_U/v_F)}}{t-L_D/v_F}=e^{i\Delta\mu\Delta L/v_F}, \tag{37}$$

so that the visibility $|\mathcal{I}_{\mathrm{AB}}|=1$, and the phase shift is $\Delta\varphi_{\mathrm{AB}}=\Delta\mu\Delta L/v_F$, in agreement with the Eq. (2).

Next, we consider a more interesting situation when the interferometer is in the weak tunneling regime (see Sec. I), and one of its arm, e.g. the upper arm of the interferometer, is much shorter than the other, $L_U \ll L_D$. Then the properties of the function $\mathcal{I}_{\mathrm{AB}}$ are determined by excitations at the lower arm of MZI at energies of order $v/L_D$. At this energies the electronic correlator in the upper arm behaves as a correlator of free fermions: $G_U(t)=1/t$. Therefore, for the visibility we obtain

$$\mathcal{I}_{\mathrm{AB}}=\int_C \frac{dt}{2\pi i}e^{i\Delta\mu t}G_D(t), \tag{38}$$

i.e. it is simply given by the Fourier transform of the electron correlation function at the edge. This leads to an interesting idea to use a strongly asymmetric MZI for the *spectroscopy of excitations* at the edge of quantum Hall system.

We now use the opportunity to analyze the role of the coupling coefficients $s_\alpha$ in this simple situation. The absolute value of the Fourier transform of the function $G_D$ is shown in Fig. 6. We see that $s_1=s_2=1/2$ is the special point. In this case, and taking the limit $u\to\infty$, the Fourier transform gives $|\mathcal{I}_{\mathrm{AB}}|=|J_0(\Delta\mu L_D/2v)|$, where $J_0$ is the zero-order Bessel function. Thus the lobes in the visibility of AB oscillations

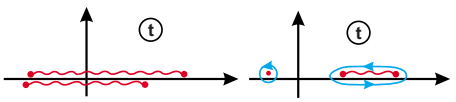


FIG. 7. (Color online) Analytic structure of the Fourier integral [Eq. (39)] in case of single biased channel (Ref. 5). Left panel: Two branch cuts (shown apart for convenience) of the integrand come from the product of two single-particle correlation functions. Right panel: In the limit $u \gg v$ two branch points corresponding to the fast mode shrink to a single pole at $t=-L_U/2v$, while the slow mode produces the branch cut going from $t=L_U/2v$ to $t=L_D/v-L_U/2v$. The blue (light gray) line shows the contour of integration $C$.

are well resolved only in the limit of strong long-range interaction. Therefore, an asymmetric MZI can be used to test the character of the interaction. From now on we assume that $s_1=s_2=1/2$.

## IV. DISCUSSION OF EXPERIMENTS

In this section we present a detailed analysis of experiments described in Sec. I. It is convenient to rewrite Eq. (36) in slightly different form by using Eq. (32) with $s_1=s_2=1/2$ and shifting the time integral:

$$\mathcal{I}_{\mathrm{AB}}(\Delta\mu)=\oint_C \frac{dt}{2\pi i}\frac{t\exp(i\Delta\mu t)}{\prod_{j,\alpha}\sqrt{(t+\Delta t-L_j/v_\alpha)}}, \tag{39}$$

where $v_1=u$ and $v_2=v$, and the contour of integration $C$ goes around the branch cuts (see, e.g., Fig. 7). These branch cuts, which replace single-particle poles of correlation functions for free electrons, originate from the interaction. On a mathematical level, they are the main source of the suppression of the coherence because at large argument $\Delta\mu$ the Fourier transform [Eq. (36)] of relatively smooth function quickly decays. We will use this fact for the analysis of dephasing. Physically, when electron tunnels, it excites two collective modes associated with two edge channels, and they carry away a part of the phase information.

On the other hand, charging effects reflected in the parameter $\Delta t$ lead to the bias-dependent shift of the AB phase, $\Delta\phi_{\mathrm{AB}}$. As it follows from Eq. (35), the phase slips by $\pi$ at points where the visibility vanishes. Away from these points, in particular at zero bias, the phase shift is a smooth function of the bias. Therefore, it is interesting to consider the value $\partial_{\Delta\mu}\Delta\phi_{\mathrm{AB}}$ at $\Delta\mu=0$, where $|\mathcal{I}_{\mathrm{AB}}|=1$, which can be found from the expansion $\mathcal{I}_{\mathrm{AB}}=|\mathcal{I}_{\mathrm{AB}}|e^{i\Delta\phi_{\mathrm{AB}}}=1+i(\partial_{\Delta\mu}\Delta\phi_{\mathrm{AB}})\Delta\mu$ in the right-hand side of Eq. (39). We find it exactly:

$$\frac{\partial\Delta\phi_{\mathrm{AB}}}{\partial\Delta\mu}=t_0-2\Delta t,\quad t_0=\frac{u+v}{2uv}(L_U+L_D), \tag{40}$$

where the first term $t_0$ is the contribution of the quantum mechanical phase accumulated due to the propagation of an electron along the MZI. The second term, found from Eq. (34), is the contribution of the charge accumulated at the arms of MZI due to the Coulomb interaction between edge channels. Partial cancellation of two effects leads to the phase rigidity found in Ref. 5. This effect is discussed below.

Finally, all the experiments found that the visibility $V_{\mathcal{G}}$ oscillates as a function of the bias $\Delta\mu$. Our model reproduces such oscillations and helps to understand their origin. Indeed, two well-defined collective modes with speeds $u$ and $v$ lead to the formation of four branch points in the integral of Eq. (39), which give relatively slowly decaying contributions. These contributions come with different bias-dependent phase factors so that the function $\mathcal{I}_{\mathrm{AB}}(\Delta\mu)$ oscillates. The period of oscillations is determined by the smallest energy scale $\epsilon$, which is given by the total size of the branch cut and can be estimated as

$$\epsilon = \frac{2uv}{(u-v)(L_U+L_D)}. \tag{41}$$

This is the general result. Later, in Secs. IV A and IV B we focus on the limit $u \gg v$, so the parameter $u$ cancels and the period of oscillations is determined by the slowest mode: $\epsilon = 2v/(L_U+L_D)$.

We would like to emphasize that oscillations in the visibility appear only when at least two modes are relatively well resolved. Our model predicts a power-law decay of the visibility. In experiments[5,6] the visibility seems to decay faster. There might be several reasons for this, e.g., low frequency fluctuations in the electrical circuit[24,25] or the electromagnetic radiation.[26] Intrinsic reasons for dephasing deserve a separate consideration. We have already mentioned that the dispersion of the Coulomb interaction, neglected here, may lead to strong dephasing.[13] However, it affects only the fast mode, while the slow mode contribution to the integral in Eq. (39) maintains the phase coherence. Therefore taken alone the dispersion of Coulomb interaction is not able to explain strong dephasing at $\nu=2$. The experiments seem to indicate that the slow mode is also dispersive, which may be a result of strong disorder at the edge, or, more interestingly, of the intrinsic structure of each edge channel.[27]

Having stressed this point, we now wish to focus solely on the phase shift and oscillations in the visibility. We use the fact that $u \gg v$ and simplify the integral in Eq. (39) by neglecting terms containing $1/u$:

$$\mathcal{I}_{\mathrm{AB}} = \oint_C \frac{dt}{2\pi i} \frac{t\exp(i\Delta\mu t)}{(t+\Delta t)\prod_j \sqrt{(t+\Delta t - L_j/v)}}. \tag{42}$$

This expression contains one pole and one branch cut (see Fig. 7). Therefore, it can be expressed in terms of the zero-order Bessel function $J_0$. After elementary steps we find

$$\mathcal{I}_{\mathrm{AB}} = e^{-i\Delta\mu\Delta t}\left[F(\Delta\mu) - i\Delta t\int_{-\infty}^{\Delta\mu} d\Delta\mu' F(\Delta\mu')\right],$$

$$F \equiv e^{i\Delta\mu t_0} J_0(\Delta\mu\Delta L/2v), \tag{43}$$

where $t_0=(L_U+L_D)/2v$, and $\Delta L=L_D-L_U$. We now proceed with the analysis of experiments discussed in Sec. I.

### A. Only one edge channel is biased

We start with the experiment.[5] Using Eqs. (17) and (19) we find

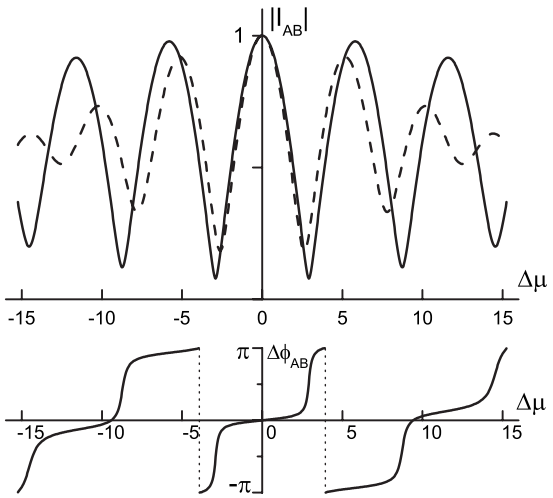


FIG. 8. The intrinsic visibility of AB oscillations $|\mathcal{I}_{\mathrm{AB}}|$ and the AB phase shift $\arg(\mathcal{I}_{\mathrm{AB}})$ in the case of a single biased channel (Ref. 5). Upper panel: The visibility is plotted as a function of the bias in units $v/L_U$ for $L_D=1.15L_U$ (solid line) and for $L_D=1.35L_U$ (dashed line). Lower panel: The phase shift is plotted for $L_D=1.15L_U$.

$$\begin{pmatrix} Q_{1j} \\ Q_{2j} \end{pmatrix} = \frac{1}{4\pi uv}\begin{pmatrix} v+u & v-u \\ v-u & v+u \end{pmatrix}\begin{pmatrix} \Delta\mu_{1j} \\ \Delta\mu_{2j} \end{pmatrix}. \tag{44}$$

In the weak tunneling regime, shown on the left panel of Fig. 2, only the outer channel in the upper arm of the interferometer is biased, $\Delta\mu_{1U}=\Delta\mu$ and $\Delta\mu_{2U}=\Delta\mu_{\alpha D}=0$. Therefore we obtain

$$Q_{1U} = \frac{u+v}{4\pi uv}\Delta\mu, \quad Q_{1D} = 0. \tag{45}$$

Then Eq. (34) gives $\Delta t = L_U(u+v)/2uv$. Substituting $\Delta t$ into Eq. (40), we find that at zero bias

$$\frac{\partial\Delta\phi_{\mathrm{AB}}}{\partial\Delta\mu} = \frac{u+v}{2uv}\Delta L. \tag{46}$$

For the symmetric interferometer, $\Delta L=0$, the phase shift is independent of the bias, away from phase slip points where the visibility vanishes. This may explain the phenomenon of phase rigidity observed in Ref. 5 if we assume that the interferometer is almost symmetric in this experiment. Indeed, the period of oscillations of the visibility is given by the energy scale [Eq. (41)]. Therefore, the overall phase shift between zeros of the visibility can be estimated as $\Delta L/(L_U+L_D) \ll 1$.

The integral in Eq. (42), evaluated numerically, is plotted in Fig. 8 for two values of the asymmetry, $L_D/L_U=1.15$ and 1.35. Our main focus is the first few oscillations of the visibility (upper panel), which reveal charging effects. We would like to emphasize several points. First, the width of the central lobe is equal to the width of the side lobes. This is because in the case of the symmetric interferometer, $L_U=L_D=L$, the branch cut shrinks to the pole (see Fig. 7) so that two poles are at $t=\pm L/2v$. Then Eq. (42) gives $|\mathcal{I}_{\mathrm{AB}}| = |\cos(\Delta\mu L/2v)|$. Note that the limit $u \gg v$ has been taken here. In general, the period of oscillations is determined by

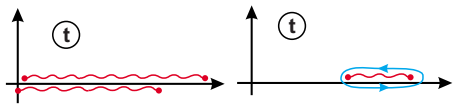


FIG. 9. (Color online) Analytic structure of the Fourier integral [Eq. (39)] in case when two edge channels are biased (Ref. 5) and in the weak tunneling regime (see Fig. 3). Left panel shows branch cuts of two single-particle correlation functions, while in the right panel the limit $u \gg v$ is taken. The branch cut extends from $t = L_U/v$ to $t = L_D/v$.

the energy scale [Eq. (41)]. Second, the small variation of the length $L_D$ of the lower arm has only a minor effect on the position of lobes, while the amplitude of oscillations is considerably suppressed. Finally, the lower panel of Fig. 8 illustrates the phenomenon of phase rigidity for almost symmetric interferometer, $L_D = 1.15 L_U$. The AB phase shift changes slowly inside the lobes and slips by $\pi$ at zeros of the visibility. All these observation are in agreement with the experiment.[5]

To conclude this section we would like to remark that the visibility in the regime of weak backscattering (see the right panel in Fig. 2) can be obtained by simply replacing $L_U$ and $L_D$. This is because in our model the charging effects are important only in the part of the MZI between two QPCs, where they induce phase shifts. For the same reason, the transparency of the second QPC does not affect the visibility.[6] In the next section we show that the symmetry between weak tunneling and weak backscattering is broken if the bias is applied to two edge channels.

### B. Two edge channels are biased

Next we analyze the experiment.[6] The details of this experiment are discussed in Sec. I. In the weak tunneling regime (see the left panel of Fig. 3) two edge channels are biased and almost completely reflected at the first QPC. Therefore, Eq. (44) gives

$$Q_{1U} = \frac{\Delta\mu}{2\pi u}, \quad Q_{1D} = 0, \tag{47}$$

and from Eq. (34) we find $\Delta t = L_U/u$.

Taking now the strong interaction limit, $u \gg v$, we find that $\Delta t \to 0$. Therefore, in the integral [Eq. (42)] the pole corresponding to the fast mode cancels (analytical structure of the integral is shown in Fig. 9), so that the visibility can be found exactly:

$$\mathcal{I}_{\mathrm{AB}} = \exp[i\Delta\mu(L_D + L_U)/2v] J_0(\Delta\mu \Delta L/2v), \tag{48}$$

where $\Delta L = L_D - L_U$. The visibility of AB oscillations, given by the absolute value of the integral [Eq. (48)], is shown in Fig. 11. One can see that in contrast to the case when only one channel is biased,[5] the central lobe is approximately two times wider than the side lobes, in agreement with the experimental observation.[6] Moreover, the width of the lobes is determined by the new energy scale, $\epsilon' = v/\Delta L$. Finally, inside the lobes the phase shift $\Delta\phi_{\mathrm{AB}} = \Delta\mu(L_D + L_U)/2v$ always grows linearly with bias so no phase rigidity should be observed.

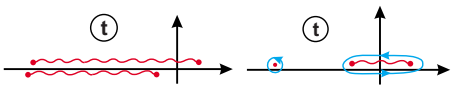


FIG. 10. (Color online) Analytic structure of the integral [Eq. (39)], same as in Fig. 9, but in the weak backscattering regime. The right panel shows the pole at $t = -(L_U + L_D)/2v$ and the branch cut, which extends from $t = -(L_D - L_U)/2v$ to $t = (L_D - L_U)/2v$.

We now switch to the regime of weak backscattering (see the right panel of Fig. 3). In the upper arm only the inner channel is biased, while only the outer channel is biased in the lower arm of the interferometer. Using again Eq. (44), we obtain

$$Q_{1U} = -\frac{u - v}{4\pi u v}\Delta\mu, \quad Q_{1D} = \frac{u + v}{4\pi u v}\Delta\mu. \tag{49}$$

Then from the Eq. (34) we find that $\Delta t = (L_D + L_U)/2v + (L_U - L_D)/2u$.

The analytical structure of the integral [Eq. (42)] is shown in Fig. 10. It looks somewhat similar to the structure shown in Fig. 7 for the case of single biased channel. However, the principal difference between these two cases is that the singularities in Fig. 10 are strongly asymmetric with respect to $t \to -t$. In order to see a consequence of this fact we take the limit $u \gg v$ and write $\Delta t = (L_U + L_D)/2v$. For the phase shift [Eq. (40)] at small bias we obtain $\partial\Delta\phi_{\mathrm{AB}}/\partial\Delta\mu = -(L_U + L_D)/2v$. Therefore, in the weak backscattering regime and when two channels are biased, no phase rigidity can be observed.

The most important new feature of the visibility (see Fig. 11) is that in contrast to the cases considered above, it grows as a function of bias around $\Delta\mu = 0$, in full agreement with the experiment.[6] It may even exceed the value 1 if two QPCs have approximately same transparencies so that $V_{\mathcal{G}}(0)$ is close to 1. This behavior may look surprising because it is expected that dephasing should suppress the visibility of AB oscillations below its maximum value [Eq. (2)] for a noninteracting coherent system. However, one should keep in mind that according to our model, oscillations of the visibility as a function of bias originate from charging effects,

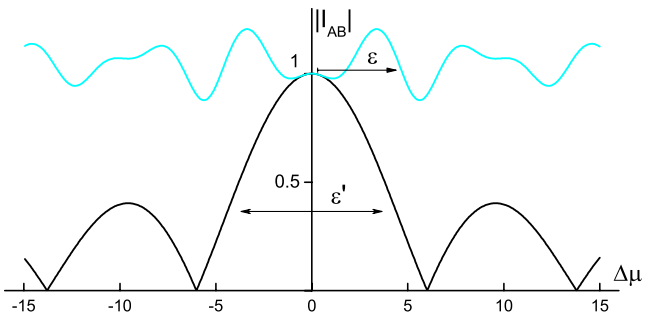


FIG. 11. (Color online) The intrinsic visibility of AB oscillations $|\mathcal{I}_{\mathrm{AB}}|$ in the case when two edge channels are biased (Ref. 6) and for strongly asymmetric interferometer, $L_D = 1.8 L_U$. It is plotted as a function of bias $\Delta\mu$ in units of $v/L_U$ for the regime of weak tunneling, black line, and for the regime of weak backscattering, blue (gray) line.

which are caused by the Coulomb interaction between edge channels. Therefore, simple arguments which rely on the Landauer formula for the conductance do not apply.

Thus in the experimental setup, where two edge channels are biased,[6] there is a strong asymmetry between weak tunneling and weak backscattering regimes, which is easily seen in Fig. 11. In order to clarify the physical origin of this effect, we evaluate the integral [Eq. (42)] in the limit of strong interaction $u \gg v$ and for a symmetric MZI, $L_U = L_D = L$. Then the branch cut shrinks to the pole, and we obtain the following simple result:

$$\mathcal{I}_{\mathrm{AB}} = \Delta t/t_0 + (1 - \Delta t/t_0) e^{i\Delta\mu t_0}, \tag{50}$$

where $t_0 = L/v$ is the time of the propagation of the slow mode between two QPCs. We find that quite similar to the result for the phase shift [Eq. (40)], here we also have a competition of two terms, $\Delta t$ given by Eq. (34) and the flight time $t_0$. Whether the visibility grows or decays depends on the sign of the second term in Eq. (50).

In the experiment[5] $\Delta t = L/2v = t_0/2$ so that the visibility always decays. On the other hand, the experiment[6] represent an intermediate case. In the regime of weak tunneling we have $\Delta t = 0$, while in the regime of weak backscattering $\Delta t = t_0$ so that in both regimes the visibility is constant for the symmetric MZI. Therefore, in Fig. 11 we had to consider a strongly asymmetric interferometer with $L_D = 1.8 L_U$. Note however, that once $\Delta t$ exceeds $t_0$ slightly, the visibility easily becomes growing function at small bias. This is exactly what happens if we relax our assumption of good screening of the interaction and allow opposite arms of the interferometer to interact. Indeed, in order to be electro-neutral the system compensates such interaction by decreasing further the charge $Q_{1U}$ below the value given by Eq. (49) so that now $\Delta t > t_0$. We have checked numerically that this assumption alone gives rise to a good agreement with the experiment[6] even in the case of symmetric interferometer.

### C. Effects of finite temperature

The temperature dependence of the visibility of AB oscillations in the MZI has been recently measured in Ref. 8. The most interesting fact is that the visibility scales exponentially with the total size of the interferometer $V_{\mathcal{G}} \propto e^{-L/l_\varphi}$. This is in obvious contradiction with the prediction $V_{\mathcal{G}} \propto e^{-\Delta L/l_\varphi}$ for free electrons,[28] where dephasing is due to energy averaging. Moreover, the coherence length scales with temperature as $l_\varphi \propto 1/T$, which does not agree with the prediction based on Luttinger liquid model for $\nu = 1$.[13,29] Here we show that the experimentally observed temperature dependence of the visibility can be explained within our model.

Indeed, according to the results of Sec. III, at high temperatures, neglecting charging effects which merely influence the prefactor, the visibility can be estimated as $V_{\mathcal{G}} \propto \int dt G_D^*(t) G_U(t)$. Here the correlators are given by the high-temperature asymptotic form [Eq. (B7)], where $X_\alpha$ has to be replaced with $L_j - v_\alpha t$. Then in the noninteracting case (i.e. for $s_1 = 1$, $s_2 = 0$, and $v_1 = v_F$) we obtain the result

$$V_{\mathcal{G}} \propto \int dt e^{-\pi T \Sigma_j |t - L_j/v_F|} \propto e^{-\pi T \Delta L/v_F}, \tag{51}$$

which agrees with the prediction in Ref. 28. On the other hand, in our model $s_1 = s_2 = 1/2$, so we obtain

$$V_{\mathcal{G}} \propto \int dt e^{-\pi T \Sigma_{\alpha,j} |t - L_j/v_\alpha|} \propto e^{-(L_U + L_D)/2 l_\varphi}, \tag{52}$$

where the dephasing length

$$l_\varphi = \frac{uv}{\pi T (u - v)}. \tag{53}$$

Thus we find that the visibility scales exponentially with the total size of the interferometer and the dephasing length scales as $l_\varphi \propto 1/T$, in full agreement with the experiment.[8]

Two remarks are in order. According to Eqs. (52) and (53), and to the results of Sec. III, the temperature dependence and the period of oscillations of the visibility are determined by the same energy scale $\epsilon$, given by Eq. (41). On the other hand, the decay of the visibility as a function of the bias $\Delta\mu$ at zero temperature is determined by a larger energy scale $\epsilon'$. It is equal to $\epsilon' = v/\Delta L$, or in case of the symmetric interferometer, it depends on the dispersion of the slow mode. The existence of two distinct energy scales, which originate from the separation of the spectrum of edge excitations on slow and fast modes, is one of the most important predictions of our theory.

Second, we note that $v$ and $u$ are the group velocities of the collective dipole and charge excitations, respectively. Very roughly, they are determined by the spatial separation between edge modes $a$ and by the distance to the back gate $D$. On the $\nu = 2$ Hall plateau, the separation $a$ grows with the magnetic field because the inner edge channel moves away from the edge of 2DEG until it disappears in the end of the plateau. Therefore, in contrast to the bare Fermi velocity, the velocity of the slow mode increases with the magnetic field. This may explain the nonmonotonic behavior of $l_\varphi$ observed in Ref. 8. Indeed, according to Eq. (53) the decoherence length first increases with the magnetic field starting from the value $l_\varphi = v/\pi T$. Then it reaches the maximum value at $v \approx u$ and goes down to the value $l_\varphi \approx u/\pi T$ on the plateau $\nu = 1$.

## V. CONCLUSION

Earlier theoretical works[25,26,28] on dephasing in MZI predicted a smooth decay of the visibility of AB oscillations as a function of temperature and voltage bias. Therefore, when Ref. 5 reported unusual oscillations and lobes in the visibility of AB oscillations as a function of bias, this was considered a great puzzle and attracted considerable theoretical attention. One of us suggested[12] a first explanation that is based on the long-range Coulomb interaction between counterpropagating edge states, which leads to resonant scattering of plasmons. Although this phenomenon may be encountered in a number of experimental situations, new experiments[6–9] unambiguously pointed to physics related to the intrinsic structure of the quantum Hall edge.

In the present paper we focus on the intrinsic properties of the edge and propose a simple model which is able to explain almost every detail of existing experiments. The key ingredient of our theory is the assumption that two chiral channels at the edge of $\nu=2$ electron system interact via the long-range Coulomb potential. This leads to a number of universalities, in particular, to the separation of the spectrum of edge excitations on slow and fast mode (plasmons) and to equal coupling of electrons to both modes. When electrons scatter off the QPCs, which play a role of beam splitters in the electronic MZI, they excite plasmons, depending on the energy provided by the voltage bias. The plasmons carry away the electronic phase information, which leads to the decay of the visibility of AB oscillations as a function of bias.

The important property of our model is that at zero temperature the phase information emitted at the first QPC can be partially recollected at the second QPC. This leads to oscillation and lobes in the visibility which can be interpreted as a size effect. The new energy scale in these oscillations, associated with the total size of the MZI and with the slow mode, determines also the temperature dependence of the visibility.

Importantly, within the framework of the same simple model we are able to explain a variety of ways the interaction effects manifest themselves in different experiments.[5–9] This includes the lobe-type structure observed in Refs. 5 and 6, the phase rigidity that was found only in Ref. 5, and the growing visibility and the asymmetry of the AB effect discovered in Ref. 6. All these phenomena can be interpreted as charging effects. Indeed, edge channels in quantum Hall systems move along the equipotential lines and can be regarded as one-dimensional metals. Therefore, they accumulate ground state charges, which lead to electronic phase shifts, depending on the bias scheme (see Figs. 2 and 3). These bias-dependent phases determine the overall AB phase shift and the specific behavior of the visibility as a function of the voltage bias.

Finally, experimentally observed decay of the visibility as a function of bias seems to be stronger than what our model predicts. We speculate that this effect cannot be explained by the long-range Coulomb interaction alone, and may originate from the dispersion of the slow mode due to disorder, or because of the intrinsic structure of each edge channel.[27] This point deserves a careful experimental and theoretical investigation. Moreover, it is interesting to find out how charging and size effects discussed here may influence the interferometry at other filling factors, where quite similar processes can take place.[30] Although the first theoretical steps have already been taken,[31–33] the experiment, as usual, may bring new surprises.

## ACKNOWLEDGMENTS

We thank A. Boyarsky and V. Cheianov for valuable discussions. We are grateful to E. Bieri, L. Litvin, S. Oberholzer, P. Roche, and C. Schönenberger for clarifying the experimental details. This work has been supported by the Swiss National Science Foundation.

## APPENDIX A: CONSISTENCY OF THE THEORY

Any model of the quantum Hall edge should satisfy the following physical conditions:[34] the existence of local electron operator, proper charge and statistics of electron operators, and the cancellation of the gauge anomaly with the one in the bulk theory. Validity of almost all of them is obvious, but it is important to ascertain that there are no intrinsic inconsistencies and incompatibilities with bulk physics in our theory. In the analysis presented below we simplify notations by omitting some indexes, and assuming the summation over repeating indexes.

Check of locality of the electron operator [Eq. (8)] is obvious,

$$[\rho_\alpha(x), e^{i\phi_\beta(x')}] = (1/2\pi)[\partial_x\phi_\alpha(x), e^{i\phi_\beta(x')}] = -\delta_{\alpha\beta}\delta(x-x')e^{i\phi_\beta(x')} \tag{A1}$$

and follows from the commutation rule for phase operators. The statistical phase $\theta$ of the operator $\psi_\alpha$ is defined as

$$\psi_\alpha(x')\psi_\alpha(x) = e^{i\theta}\psi_\alpha(x)\psi_\alpha(x'). \tag{A2}$$

Using the simple relation

$$e^{i\phi_\alpha(x')}e^{i\phi_\alpha(x)} = e^{-[\phi_\alpha(x'),\phi_\alpha(x)]}e^{i\phi_\alpha(x)}e^{i\phi_\alpha(x')}$$

and the commutation relation for bosonic phase operators we find that our electron operators [Eq. (8)] are fermions with the phase $\theta=\pi$. Finally, the total charge at the quantum Hall edge is

$$q = \sum_\beta \int dx\rho_\beta(x) = (1/2\pi)\sum_\beta \int dx\partial_x\phi_\beta(x).$$

Therefore, using relation (A1) we find

$$[q, \psi_\alpha(x)] = -\psi_\alpha(x), \tag{A3}$$

which means that the fermion [Eq. (8)] in our model has an electron charge, $e=1$.

The only nontrivial question is whether the condition of the cancellation of the anomaly inflow imposes any constraint on the interaction matrix $V_{\alpha\beta}$. The answer is no. To show this we use the Chern-Simons action for the gauge field $a_\mu$ in the effective low-energy description of quantum Hall bulk physics[34] at $\nu=2$:

$$S_{\mathrm{CS}} = \int dt \int_\Omega d^2x \varepsilon_{\mu\nu\lambda} a_{\alpha\mu}\partial_\nu a_{\alpha\lambda}. \tag{A4}$$

Here $\Omega$ is the region of 2DEG where the quantum Hall liquid is present. After the gauge transformation $a_{\alpha\mu}\to a_{\alpha\mu}+\partial_\mu\lambda_\alpha$ the gauge anomaly (total change of action) acquires the following form:

$$\delta S_{\mathrm{CS}} = \int dt \int_{\partial\Omega} dx\lambda_\alpha(\partial_t a_{\alpha x} - \partial_x a_{\alpha t}). \tag{A5}$$

In our model the action for edge excitations alone can be written as

$$S = \int dt \int_{\partial\Omega} dx(\partial_x\phi_\alpha\partial_t\phi_\alpha - V_{\alpha\beta}\partial_x\phi_\alpha\partial_x\phi_\beta).$$

The point is that for *any* interaction matrix $V_{\alpha\beta}$ the coupling of edge modes with the field $a_\mu$ may be written in the gauge invariant form

$$S(a) = \int \int_{\partial\Omega} dxdt(D_x\phi_\alpha D_t\phi_\alpha - V_{\alpha\beta}D_x\phi_\alpha D_x\phi_\beta - \epsilon_{\mu\nu}a_{\alpha\mu}\partial_\nu\phi_\alpha), \tag{A6}$$

where $D_\mu\phi_\alpha = \partial_\mu\phi_\alpha - a_{\alpha\mu}$. After the gauge transformation in the edge action, $\phi_\alpha \to \phi_\alpha + \lambda_\alpha$, the anomaly [Eq. (A5)] cancels in the total action $S_{\mathrm{CS}} + S(a)$.

## APPENDIX B: CALCULATION OF ELECTRON CORRELATION FUNCTION

After we have introduced the model in Sec. II, the derivation of the electronic correlation function is relatively simple. We represent the electronic operators as $\psi_{1j} \propto e^{i\phi_{1j}}$ and fix the normalization in the end of calculations. Using the Gaussian character of the theory, we write

$$i\langle\psi_{1j}^\dagger(x,t)\psi_{1j}(0,0)\rangle \propto \exp(i\Delta\mu_{1j}t - 2\pi i Q_{1j}x)K_j(x,t), \tag{B1}$$

where the first term is the average zero-mode contribution, while the function $K_j$ is the fluctuation part:

$$\log[K_j(x,t)] = \langle[\phi_{1j}(x,t) - \phi_{1j}(0,0)]\phi_{1j}(0,0)\rangle. \tag{B2}$$

Switching to the basis which diagonalizes the Hamiltonian [Eq. (24)] we write

$$\phi_{1j}(x,t) = i\sum_{\alpha,k}\sqrt{\frac{2\pi}{Wk}}[S_{1\alpha}b_{\alpha j}(k)e^{ikX_\alpha} + S_{1\alpha}^* b_{\alpha j}^\dagger(k)e^{-ikX_\alpha}], \tag{B3}$$

where we introduced the notation

$$X_\alpha \equiv x - v_\alpha t$$

and neglected fluctuations of zero modes because we are about to take the thermodynamic limit, $W \to \infty$. Substituting this expression for the phase operator into the Eq. (B2), we obtain,

$$\log[K_j] = \sum_\alpha s_\alpha \int_0^\Lambda \frac{dk}{k}\{n_\alpha(k)(e^{-ikX_\alpha} - 1) + [1 + n_\alpha(k)](e^{ikX_\alpha} - 1)\}, \tag{B4}$$

where $n_\alpha(k) = [\exp(\beta v_\alpha k) - 1]^{-1}$ are the boson occupation numbers, $\Lambda$ is the ultraviolet cutoff, and $s_\alpha = |S_{1\alpha}|^2$.

The best way to proceed is to expand occupation numbers in Boltzmann factors, $n_\alpha(k) = \Sigma_{m=1}^\infty \exp(-\beta v_\alpha mk)$, and integrate each term separately. This gives

$$\log[K_j] = -\sum_\alpha s_\alpha \sum_{m=-\infty}^{\infty} \log[\Lambda(i\beta v_\alpha m - X_\alpha)]. \tag{B5}$$

Combining this result with Eq. (B1), we finally obtain

$$i\langle\psi_{1j}^\dagger(x,t)\psi_{1j}(0,0)\rangle = \exp(i\Delta\mu_{1j}t - 2\pi i Q_{1j}x) \times \prod_\alpha \{(v_\alpha/\pi T)\sinh[\pi T X_\alpha/v_\alpha]\}^{-s_\alpha}, \tag{B6}$$

where the prefactor is chosen to be consistent with the free fermion case for $s_1 = 1$ and $s_2 = 0$. In the zero-temperature limit, $T = 0$, we obtain correlator (30). At high temperatures, $T \gg |X_\alpha|/v_\alpha$ the correlator scales as

$$i\langle\psi_{1j}^\dagger(x,t)\psi_{1j}(0,0)\rangle \propto \exp\left[-\sum_\alpha \pi T s_\alpha |X_\alpha|/v_\alpha\right]. \tag{B7}$$


[1] *The Quantum Hall Effect*, edited by R. E. Prange and S. M. Girvin (Springer, New York, 1987).
[2] S. Datta, *Electronic Transport in Mesoscopic Systems* (Cambridge University Press, Cambridge, 1999).
[3] For a review, see, A. M. Chang, Rev. Mod. Phys. **75**, 1449 (2003); X.-G. Wen, Adv. Phys. **44**, 405 (1995).
[4] Y. Ji, Y. Chung, D. Sprinzak, M. Heiblum, D. Mahalu, and H. Shtrikman, Nature (London) **422**, 415 (2003).
[5] I. Neder, M. Heiblum, Y. Levinson, D. Mahalu, and V. Umansky, Phys. Rev. Lett. **96**, 016804 (2006).
[6] E. Bieri, Ph.D. thesis, University of Basel, 2007; E. Bieri (unpublished).
[7] Preden Roulleau, F. Portier, D. C. Glattli, P. Roche, A. Cavanna, G. Faini, U. Gennser, and D. Mailly, Phys. Rev. B **76**, 161309(R) (2007).
[8] P. Roulleau, F. Portier, D. C. Glattli, P. Roche, A. Cavanna, G. Faini, U. Gennser, and D. Mailly, Phys. Rev. Lett. **100**, 126802 (2008).
[9] L. V. Litvin, H.-P. Tranitz, W. Wegscheider, and C. Strunk, Phys. Rev. B **75**, 033315 (2007); L. V. Litvin, A. Helzel, H.-P. Tranitz, W. Wegscheider, and C. Strunk, arXiv:0802.1164, Phys. Rev. B (to be published).
[10] I. Neder, F. Marquardt, M. Heiblum, D. Mahalu, and V. Umansky, Nat. Phys. **3**, 534 (2007).
[11] M. Büttiker, Phys. Rev. Lett. **57**, 1761 (1986).
[12] E. V. Sukhorukov and V. V. Cheianov, Phys. Rev. Lett. **99**, 156801 (2007).
[13] J. T. Chalker, Y. Gefen, and M. Y. Veillette, Phys. Rev. B **76**, 085320 (2007).
[14] I. Neder and E. Ginossar, Phys. Rev. Lett. **100**, 196806 (2008).
[15] S.-C. Youn, H.-W. Lee, and H.-S. Sim, Phys. Rev. Lett. **100**, 196807 (2008).
[16] In Fig. 1 of Ref. 5 the counter-propagating edge state goes from the source S3 to QPC0 and under the air bridge comes very closely to the upper arm of the interferometer, which is the part of the channel between QPC1 and QPC2.
[17] P. Roche (private communication).
[18] D. B. Chklovskii, B. I. Shklovskii, and L. I. Glazman, Phys. Rev. B **46**, 4026 (1992).
[19] X.-G. Wen, *Quantum Field Theory of Many-Body Systems* (Ox-

ford University Press, Oxford, 2004).
[20] Th. Giamarchi, *Quantum Physics in One Dimension* (Oxford University Press, Oxford, 2003).
[21] L. D. Landau and E. M. Lifshits, *Theoretical Physics* (Butterworth-Heinemann, Oxford), Vol. 8.
[22] Note that $\Delta\mu_{\alpha j}$ is the electrochemical potential because our definition [Eq. (11)] contains a single-particle contribution.
[23] G. D. Mahan, *Many Particle Physics*, 2nd ed. (Plenum, New York, 1993).
[24] G. Seelig and M. Büttiker, Phys. Rev. B **64**, 245313 (2001).
[25] G. Seelig, S. Pilgram, A. N. Jordan, and M. Büttiker, Phys. Rev. B **68**, 161310(R) (2003).
[26] F. Marquardt and C. Bruder, Phys. Rev. Lett. **92**, 056805 (2004); Phys. Rev. B **70**, 125305 (2004).
[27] J. Fröhlich, B. Pedrini, Ch. Schweigert, and J. Walcher, J. Stat. Phys. **103**, 527 (2001).
[28] V. S.-W. Chung, P. Samuelsson, and M. Büttiker, Phys. Rev. B **72**, 125320 (2005).
[29] For earlier works on dephasing in one-dimensional interacting systems, see K. Le Hur, Phys. Rev. Lett. **95**, 076801 (2005), and references therein.
[30] C. L. Kane, M. P. A. Fisher, and J. Polchinski, Phys. Rev. Lett. **72**, 4129 (1994).
[31] K. T. Law, D. E. Feldman, and Y. Gefen, Phys. Rev. B **74**, 045319 (2006).
[32] V. V. Ponomarenko and D. V. Averin, Phys. Rev. Lett. **99**, 066803 (2007).
[33] E. Ardonne and E.-A. Kim, J. Stat. Mech.: Theory Exp. (2008) L04001; B. J. Overbosch and X.-G. Wen, arXiv:0706.4339 (unpublished); B. Rosenow, B. I. Halperin, S. H. Simon, and Ady Stern, Phys. Rev. Lett. **100**, 226803 (2008); W. Bishara and C. Nayak, Phys. Rev. B **77**, 165302 (2008).
[34] J. Fröhlich and A. Zee, Nucl. Phys. B **364**, 517 (1991); J. Fröhlich and T. Kerler, *ibid.* **354**, 369 (1991).